http://dx.doi.org/10.5012/bkcs.2012.33.10.3355

Photovoltaic Efficiencies on Dye-Sensitized Solar Cells Assembled with Graphene-Linked TiO_2 Anode Films

A-Young Kim, Jieun Kim, Min Young Kim,† Seung Won Ha,† Ngyen Thi Thuy Tien,† and Misook Kang*

Department of Chemistry, College of Science, Yeungnam University, Gyeongsan, Gyeongbuk 712-749, Korea
**E-mail: mskang@ynu.ac.kr*
†Korea Science Academy of Korea Advanced Institute of Science and Technology, Busan 614-822, Korea
Received June 14, 2012, Accepted July 19, 2012

To promote the photoelectric conversion efficiency of dye-sensitized solar cells (DSSCs), graphene is introduced as a working electrode with TiO_2 in this study, because it has great transparency and very good conductivity. XRD patterns indicate the presence of graphene and TiO_2 particles in graphene-linked TiO_2 samples. Moreover, TEM pictures also show that the nano-sized TiO_2 particles are highly dispersed and well-linked onto the thin layered graphene. On the basis of the UV-visible spectra, the band gaps of TiO_2, 1.0 wt % graphene-TiO_2, 5.0 wt % graphene-TiO_2, and 10.0 wt % graphene-TiO_2 are 3.16, 2.94, 2.25, and 2.11 eV, respectively. Compared to pure TiO_2, the energy conversion efficiency was enhanced considerably by the application of graphene-linked TiO_2 anode films in the DSSCs to approximately 6.05% for 0.1 wt % graphene-TiO_2 with N719 dye (10.0 mm film thickness and 5.0 mm × 5.0 mm cell area) under 100 mW/cm^2 of simulated sunlight. The quantum efficiency was the highest when 1.0 wt % of graphene was used. In impedance curves, the resistance was smallest for 1.0 wt % graphene- TiO_2-DSSC.

Key Words : Graphen, Graphene-linked TiO_2, Dye-sensitized solar cells, Energy conversion efficiency, Impedance

Introduction

In order to enhance the photovoltaic efficiency of dye-sensitized solar cells (DSSC), electrons, which are transferred from the LUMO of dye molecules, should be accepted easily and donated to the external surface of the semiconductor film[1-5] as shown in Scheme 1. However, a limitation is imposed by the loss of electrons that are moved and then dropped down onto a spherical surface of a semiconductor film. The electron is expected to migrate rapidly to the surface of a defected semiconductor film that is well-arranged by self assembly with electron capturing and donating properties and converted into an FTO-conducting electrode without electron loss, thereby increasing the energy conversion efficiency.

Here, in order to absorb as much sun-light as possible and to easily donate the captured electrons from dye molecules to the external surface of the semiconductor film, we have tried to introduce graphene as a DSSC-electrode in this study. Graphene has gained lots of attention lately due to its newly discovered amazing and unique characteristics. It is well-known as an allotrope of carbon, a sheet of honeycombed linked carbon atoms, with a C-C bond length of 0.142 nanometers.[6-8] It has some special features that make it optimal for photochemical devices such as solar cells, because it has great transparency and very good conductivity with low resistance- only 10^{-6} Ω·cm/sheet. Though it absorbs very little in the visible range, an absorbance of only 2.3% of incident white light, graphene has increased possible absorption in the UV range of longer wavelengths, resulting in graphene acting as a UV stabilizer. Moreover, the energy gap of graphene can be tuned and scales inversely with the width, despite the fact that initially there is no band gap, a main drawback of graphene. In addition, at room temperature, it has exceptionally high electron mobility, greater than 15,000 cm^2/Vs. On the basis of these properties, recently, graphene has been applied to photocatalysis.[9-11] Particularly, Zhang *et al.*[9] reported photocatalytic activity for hydrogen evolution on TiO_2/graphenenanocomposites. An enhancement of photocatalytic hydrogen evolution was observed over the TiO_2/GS composite photocatalysts: 1.6 times larger for TiO_2/2.0 wt % GS than that of Degussa P25. However, cases have so far rarely been applied to DSSC and more detailed study is thus required.

Graphene is a great candidate due to its interesting characteristics, especially in the electrochemistry field, and we

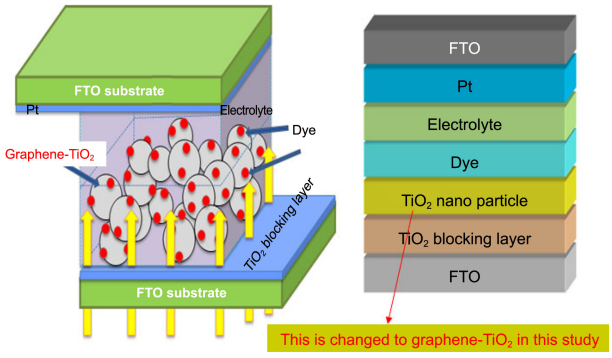

Scheme 1. Cell assembly configuration of the photovoltaic efficiency of dye-sensitized solar cells (DSSC).

associated graphene with original TiO_2 and searched for the best combination. Graphene (1.0, 5.0, 10.0 wt %)-linked TiO_2 was synthesized in this study. The synthesized samples were characterized by X-ray diffraction (XRD), transmission electron microscopy (TEM), UV-visible spectroscopy, and impedance analysis. The photovoltaic performance of the grephen-TiO_2/dye (N719) solar cell was evaluated from the overall conversion efficiency, fill factor (FF), V_{oc} and J_{sc}. In addition, the efficiency was compared with that of a pure TiO_2 sample prepared using the same synthesis method.

Experimental Section

Preparation of Graphene and Graphene-Linked TiO_2. For the preparation of graphene, graphite oxide should first be made[12,13]: 6.0 g of graphite powder was added to 300.0 mL of concentrated H_2SO_4 at a temperature of 0 °C with stirring for 2 h and sonicating for 1 h. Into the mixture, 24.0 g of $KMnO_4$ was infused maintaining temperature at < 10, followed by an hour at 35 °C. After cooling, 100.0 mL of distilled water for dilution was poured into the mixture, and it was washed by 300.0 mL H_2O. 80.0 mL of 30% H_2O_2 was dropped into the mixture, and then the precipitation was washed with 1.0 L of 5% HCl and 4.0 L of H_2O. The product (graphite oxide) was dried at 60 °C for 24 h. The prepared graphite oxide (0.5 g) in the previous step was put in 300 mL of ethylene glycol with stirring, followed by sonication for 2 h. As a reducing agent, 0.5 mL of hydrazine hydrate was dropped slowly into the mixture and stirred overnight. The final mixture was thermally treated in an autoclave at T = 300, and the obtained precipitate was washed first with ethanol 3 times and H_2O for five times, and lastly with ethanol again. The product (graphene) was dried at 60 °C for 24 h. Graphene-linked TiO_2 with various mol fractions of graphene (1.0, 5.0, and 10.0 wt %) was then prepared. 10.0 g of titanium tetraisopropoxide (TTIP, 99.95%, Junsei Chemical, Japan) was added to a beaker of 200.0 mL H_2O. Based on the weight % graphene (1.0, 5.0, and 10.0 wt %), the graphite oxide was added to the mixed solution, and was then sonicated for 1 h. 1.0 mL of hydrazine hydrate was dropped into the mixture and stirred for 5 h. This mixture was transferred into an autoclave and thermally treated at a temperature of 180 °C for 6 h. The obtained compounds were washed with ethanol and water and dried at 60 °C for 24 h. Finally, for comparison, pure nano-sized TiO_2 particles were synthesized by a commercialized solvothermal method.[14]

Characteristics of Graphene and Graphene-TiO_2s. The synthesized graphene and graphene-linked TiO_2s powders were examined by XRD (MPD, PANalytical, at Yeungnam University Instrumental Analysis Center) with nickel-filtered CuKα radiation (30 kV, 30 mA) at 2θ angles ranging from 10 to 80°, a scan speed of 10° min^{-1} and a time constant of 1 s. The sizes and morphologies of the graphene and graphene-linked TiO_2 particles were measured by TEM (H-7600, Hitachi, at Yeungnam University Instrumental Analysis Center) operated at 120 kV. The solid-UV-visible spectra of the graphene and graphene-linked TiO_2 particles were obtained using a Cary 500 spectrometer with a reflectance sphere over the special range of 200 to 800 nm. TGA measurements of graphite and graphene were collected using a PerkinElmer TGA instrument equipped with a platinum crucible. Samples were heated from room temperature to 900 °C with a heating rate of 10 °Cmin^{-1} while the chamber was continuously purged with O_2 gas at a rate of 25 mL/min.

Manufacturing Dye-Sensitized Solar Cells (DSSCs) Assembled with Graphene-Linked TiO_2. To manufacture dye-sensitized solar cells (DSSCs), a paste of the graphene-linked TiO_2 was produced by mixing 2.0 g of graphene-TiO_2 powders with a mixture consisting of 5.0 g of α-tepinol, 0.5 g of cellulose, and 20 mL of ethanol, after sonication for 24 h at 1200 Wcm^{-2}. A graphene-TiO_2 film was fabricated by coating onto an FTO conducting glass plate (Hartford FTO, ~30 $ohmcm^{-2}$, 80% transmittance in visible region) using a squeeze printing technique. The film was treated by heating at 450 °C for 30 minutes to remove the additives. For DSSC manufacture, the prepared thin film electrode was immersed in a 3.0×10^{-4} M N719 dye solution at room temperature for 2 h, rinsed with anhydrous ethanol and dried. A Pt-coated FTO electrode was placed over the dye-adsorbed graphene-TiO_2 electrode, and the edges of the cell were sealed with a sealing sheet (PECHM-1, Mitsui-Dupont Polychemical). The redox electrolyte consisted of 0.5 mol KI, 0.05 mol I_2, and 0.5 mol 4-*tert*-butylpyridine as a solvent. The photocurrent-voltage (I-V) curves were used to calculate the J_{sc}, V_{oc}, FF, and overall conversion efficiency of the graphene-TiO_2-DSSCs. I-V curves were measured under white light irradiation from a xenon lamp (max. 150W) using a sun 2000 solar simulator (ABE technology). The light intensity was adjusted with a Si solar cell for approximated AM-1.5 radiation. The incident light intensity and active cell area were 100 $mWcm^{-2}$ (one sun illumination) and 0.25 cm^2 (0.5 × 0.5 cm), respectively.

The AC-impedance measurements were performed with a potentiostat-galvanostat equipped with a ComPactStat electrochemical interface from IVIUM technology under constant light illumination of 100 $mWcm^{-2}$. EIS of the graphene-TiO_2-DSSCs was performed under constant light illumination and open-circuit conditions. The applied bias voltage and AC-amplitude were set at open-circuit voltage of the graphene-TiO_2-DSSCs and 10 mV between the FTO/Pt counter electrode and the FTO/graphene-TiO_2/dye working electrode, respectively. The frequency range explored was 0.1-100 kHz.

Results and Discussion

Characteristics of Graphene and Graphene-TiO_2. For preparation of the graphene-TiO_2, we synthesized graphite oxide and graphene as mentioned in experimental section. Figure 1 shows the XRD patterns and TEM images of the graphite oxide and graphene powder. The graphite oxide displays a (001) diffraction peak at $2\theta = 11.1°$ [15] as shown in figure a). After the reduction of graphite oxide by hydrazine

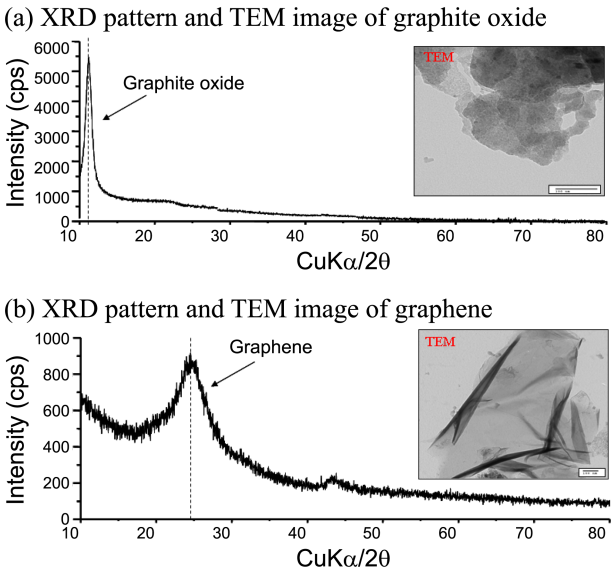

Figure 1. XRD patterns and TEM images of the graphite oxide and graphene powders.

hydrate to transfer the graphene, a new (002) diffraction peak appears at about 2θ = 24.1° corresponding to an inter-planar distance of 0.42 nm as shown in Figure b). This means that the periodic structure of graphite oxide was eliminated and the conjugated graphene network was successfully established with forms of thin layered nano-sheet as shown in TEM photos.

To identify the thermal stability of graphene, TG analysis was conducted. As shown in Figure 2, with increasing temperature, graphite oxide starts to degrade at low temperature. The weight losses are attributed to the evaporation of absorbed small molecules like water with exothermic decomposition until 170 °C, and the decomposition of the residual oxygen-containing functional groups in the region of 170-550 °C, since chemical reduction of graphite oxide usually results in incompletely reduced products. For graphene, the weight loss was not determined until 480 °C, and then there was loss in the region of 480-700 °C, which was ascribed to main-chain pyrolysis with combustion. Notably, the graphene can remain stable, since the graphene-TiO_2 film is treated by heating at 450 °C for 30 minutes to remove the additives in a step of assembling the DSSCs.

Figure 3 shows the XRD patterns of the 1.0, 5.0, and 10.0 wt % graphene-TiO_2 and pure TiO_2. Without thermal treatment above 500 °C, the graphene-TiO_2 exhibited an anatase structure. The anatase structure showed peaks at 25.3, 38.0, 48.2, 54, 63, and 68° 2θ, which were assigned to the (d_{101}), (d_{004}), (d_{200}), (d_{105}), (d_{211}), and (d_{204}) planes, respectively.[16] However, the peak intensity at most of the planes decreased slightly with increasing graphene content compared to that of pure TiO_2. Generally, the crystalline domain sizes decrease with increasing line-broadening of the peaks. The line broadening of the peak of the A (101) index is related to the size of the hexagonal crystalline phase. Scherrer's equation, $t = 0.9\lambda/\beta\cos\theta$, was used to estimate the crystalline domain size, where λ is the wavelength of the incident X-rays, β is

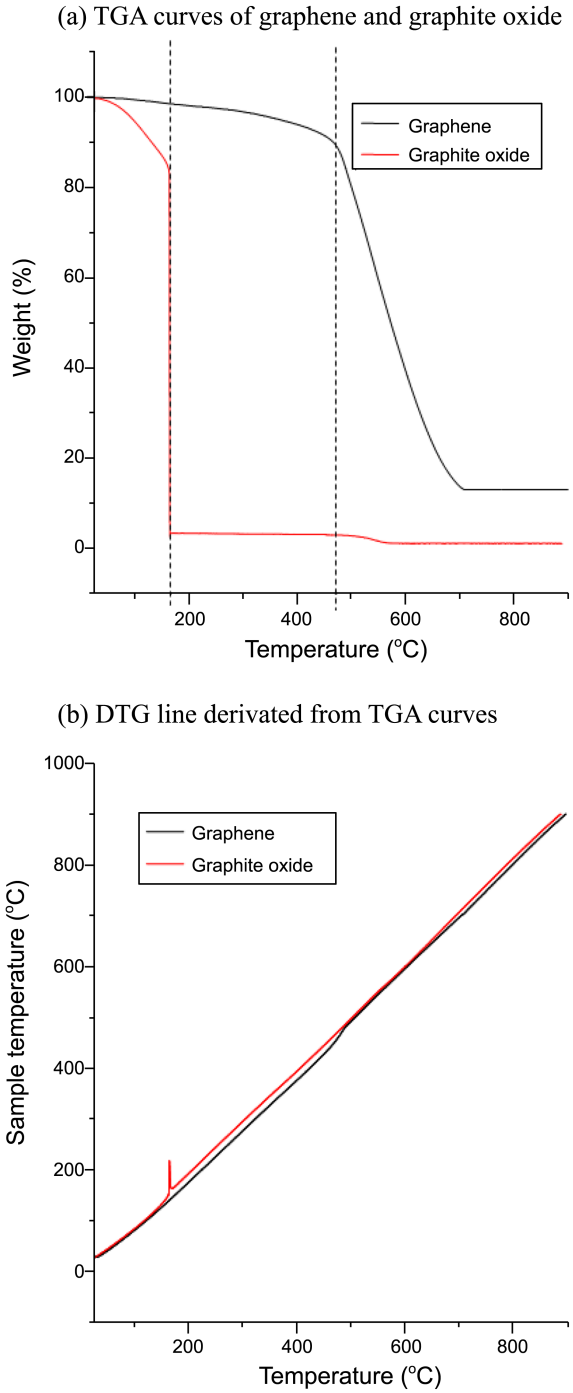

Figure 2. TG analysis to identify the thermal stability of graphene.

the full width at half maximum (FWHM) height in radians, and θ is the diffraction angle. When the FWHM of the peak at 25.3° 2θ was selected, the calculated crystalline domain sizes were 33, 27, 25, and 21 nm for TiO_2 and 1.0, 5.0, and 10.0 wt % graphene-TiO_2s, respectively.

Figure 4 shows TEM images of the particle shapes of TiO_2 and 10.0 wt % graphene-TiO_2. A relatively uniform mixture of rhombic and spherical particles with sizes ranging from 10 to 20 nm was observed in the TiO_2 particles. Surprisingly, when graphene was added to the TiO_2, it was confirmed that TiO_2 nano-particles were highly and stably dispersed over

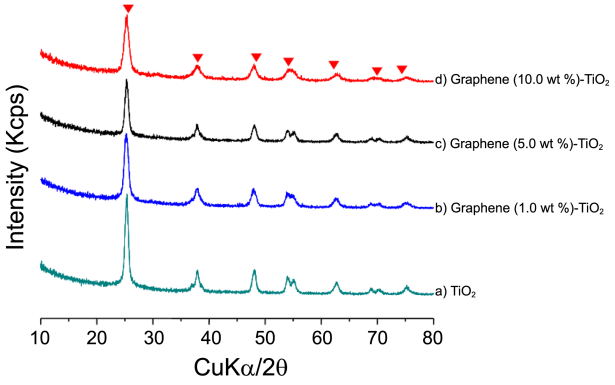

Figure 3. XRD patterns of pure TiO_2 and graphene-TiO_2 synthesized.

the surface of the nano-sheet of graphene. This result means that the graphene was well-linked to the TiO_2 chemically.

The UV-visible spectra of the 1.0, 5.0, and 10.0 wt % graphene-TiO_2 and pure TiO_2 powders were obtained to determine the relationship between the solar energy conversion efficiency and the spectroscopic properties. The absorption band for the octahedral symmetry of Ti^{4+} normally appears at approximately 350-380 nm. In the spectra of graphene-TiO_2, the absorption bands were slightly shifted to a longer wavelength compared to pure TiO_2, and the broadened tail may indicate a graphene component. The absorption coefficient is given by the following equation, which is often called the Tauc law[17]: $(\alpha h\nu)^{1/2} = \beta(h\nu - E_g)$, where E_g is the Tauc optical band gap, $\alpha = 2.303A/d$ (A: optical density and d: thickness of the sample), ϖ is the incident light angular frequency and is a parameter depending on the transition type of the absorption edge. β is a constant that depends on the width of the localized states in the band gap. The plot of $\alpha h\nu$ *vs* $h\nu$ of TiO_2 and graphene-TiO_2 are shown in Figure 5. The intercept of the abscissa axis with the full line of the $(\alpha h\nu)^{1/2}$ *vs* $h\nu$ plot allows the determination of optical band gap. The band gaps obtained by extrapolation using the Tauc's equation[17] in pure TiO_2, 1.0, 5.0, and 10.0 wt % graphene-TiO_2 were about 3.16, 2.94, 2.25, and 2.11 eV, respectively. Band gaps in semiconductor materials are closely related to the wavelength range absorbed, where the band gap decreases with increasing absorption wavelength.

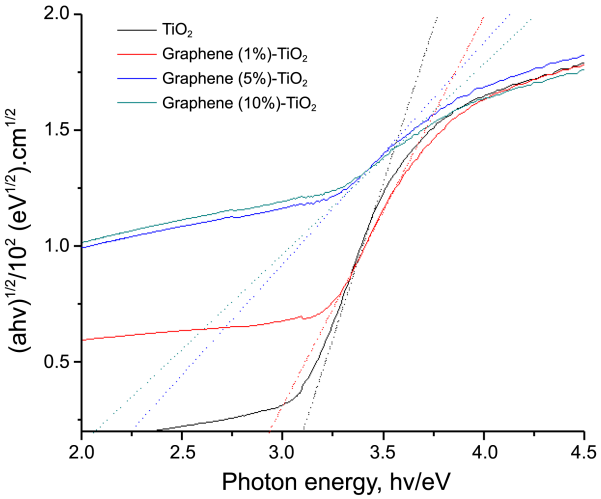

	TiO_2	Graphene (1%)-TiO_2	Graphene (5%)-TiO_2	Graphene (10%)-TiO_2
Bandgap (eV)	3.16	2.94	2.25	2.11

Figure 5. UV-visible spectra of pure TiO_2 and graphene-TiO_2.

As graphene plays an important role of electron receiving and giving in DSSCs, and its light absorption is therefore important, the electron transfer is more crucial to enhance the DSSC performance.

Photovoltaic Performance of Graphene-TiO_2-DSSC. The photoelectric properties were measured using a voltmeter and ampere meter (Model 2000, Keithley) with a variable load. A voltmeter above power failure and a lock-in amplifier were used. A 150 W illuminant Xenon lamp was employed as a radiation source at an AM-1.5 radiation angle. The light intensities were measured using a power analyzer and thermal smart-sensor. The *FF* and solar energy conversion efficiency (η) were calculated according to Eqs. (1) and (2), respectively.

$$FF = I_{max} \times V_{max} / I_{sc} \times V_{oc} \quad (1)$$

$$\eta\,(\%) = P_{out}/P_{in} \times 100 = I_{max} \times V_{max}/P_{in} \times 100 = I_{sc} \times V_{oc} \times FF \quad (2)$$

Figure 6 shows the photocurrent-voltage curves of the

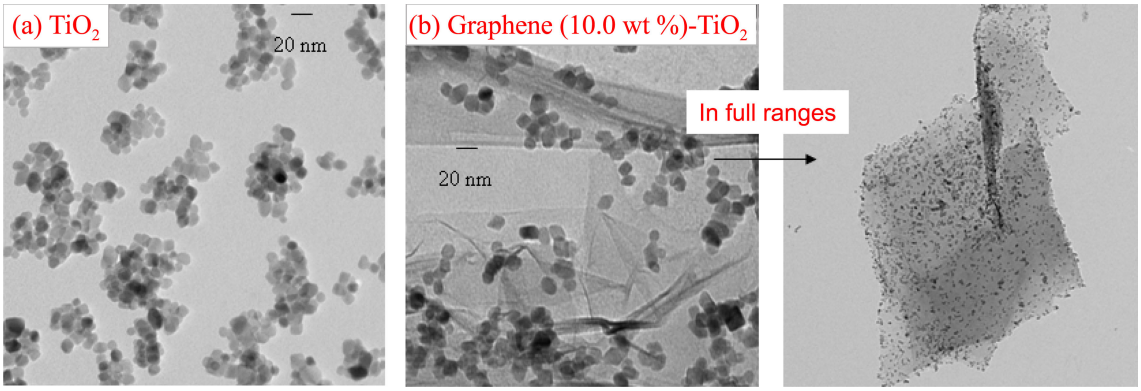

Figure 4. TEM images of pure TiO_2 and graphene-TiO_2.

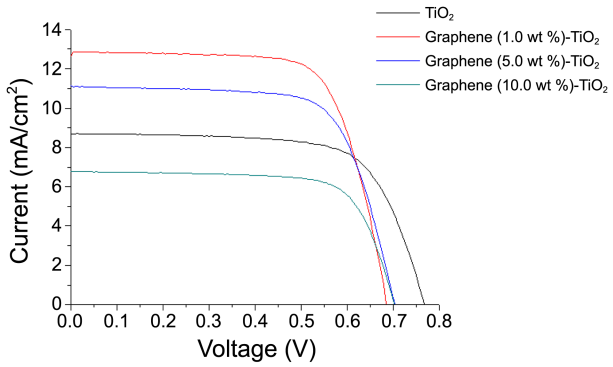

Sample	V_{oc} (V)	J_{sc} (mA/cm^2)	Fill factor	Efficiency (%)
TiO_2	0.77	8.69	0.66	4.42
Graphene (1.0 wt %)-TiO_2	0.68	12.89	0.69	6.05
Graphene (5.0 wt %)-TiO_2	0.71	11.15	0.66	5.22
Graphene (10.0 wt %)-TiO_2	0.70	6.75	0.70	3.31

Figure 6. Solar energy conversion efficiency of the DSSCs fabricated with pure TiO_2 and graphene-TiO_2.

DSSCs assembled with the pure TiO_2 and the 1.0, 5.0, and 10.0 wt % graphene-TiO_2. The FF, V_{oc}, J_{sc}, and overall energy efficiency were determined as described above. The film thickness was in the range of 8.0-10.0 mm and the unit cell area was fixed with dimensions of 5.0 mm × 5.0 mm. A DSSC assembled with pure TiO_2 had a V_{oc} of 0.77 V and a J_{sc} of 8.69 mAcm^{-2} at an incident light intensity of 100 mW/cm^2. The power conversion efficiency was 4.42% for the pure TiO_2 anatase structure, but increased to 6.05% in the DSSC made from 1.0 wt % graphene-TiO_2 film, with a J_{sc} of 12.89 mAcm^{-2} and a V_{oc} of 0.68 V. On the other hand, the efficiency was slightly reduced in the DSSC made with a graphene content > 10.0 wt %, which confirmed that graphene-TiO_2 is a better material in DSSCs than pure TiO_2.

The EIS results of graphene-TiO_2-DSSCs are presented by Nyquist plots in Figure 7. In general, the impedance spectrum of the DSSC shows three semicircles in the frequency range of 0.1-100 kHz. The first semicircle, R_{ct1}, is related to the charge transfer at the counter electrode measured in the kHz range. The second semicircle, R_{ct2}, is related to the electron transport at the graphene-TiO_2/dye/electrolyte interface in the range of 1-100 Hz. The third semicircle, Z_w, shows the Warburg diffusion process of I/I^3 in the electrolyte, measured in the mHz range.[18] Otherwise, the ohmic serial resistance (R_s) is associated with the series resistance of the electrolytes and electric contacts in the DSSC. These three semicircles indicate the R_{ct1}, R_{ct2} and Z_w of an equivalent circuit, as shown under the table. The second semicircle decreased significantly due to the effects of the doping of graphene. The TiO_2-DSSC and 10.0 wt % graphene-TiO_2-DSSC appeared to have a higher total resistance in the current path across the device than that of the 1.0 and 5.0 wt % graphene-TiO_2-DSSCs. Notably, R_{ct2} was largely decreased in the cell assembled with the 1.0 wt % graphene-TiO_2-DSSC compared to that of the pure TiO_2-DSSC. It is notable that the electron flow from the LUMO of the dye to the FTO through the conduction band of graphene-TiO_2 became more efficient. In the case of the first and third semicircles, four DSSCs showed similar values because the preparation conditions of counter electrodes were the same. The Rs related to the sheet resistance of the FTO did not show any significant change because the same FTO glasses were used in all samples. Therefore, it is notable that the electron charge transfer improved at the semiconductor/dye/electrolyte interface due to the effects of graphene dopant into TiO_2.

IPCE in Figure 8 indicates the number of incident photons inside the cell and their contribution to the efficiency.[19] IPCE is defined as the ratio of the number of electrons in the external circuit produced by an incident photon at a given wavelength. DSSCs that primarily respond to the wave-

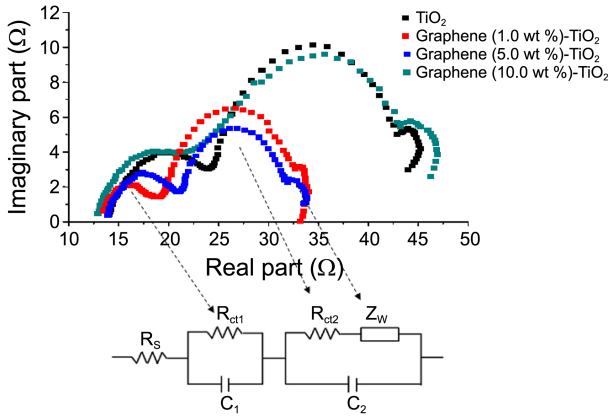

Sample	R_s	R_{ct1}	R_{ct2}	Z_w	R_t
TiO_2	14.02	9.13	19.74	2.31	45.20
Graphene (1.0 wt %)-TiO_2	14.02	6.35	11.05	2.15	33.57
Graphene (5.0 wt %)-TiO_2	13.46	4.86	14.06	1.63	34.01
Graphene (10.0 wt %)-TiO_2	12.96	8.22	21.33	4.39	46.90

Figure 7. Impedance curves of the DSSCs fabricated with pure TiO_2 and graphene-TiO_2.

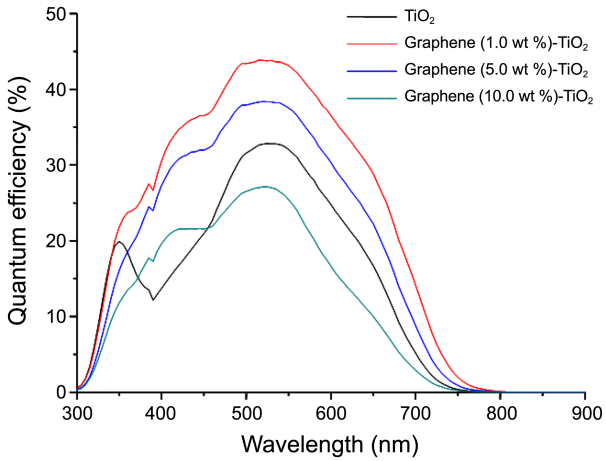

Figure 8. IPCE curves of the DSSCs fabricated with pure TiO_2 and graphene-TiO_2.

length of visible light were measured in the 300-800 nm region. The dye that reacted at a wavelength of 500-600 nm had the highest quantum number, which is corresponding to the absorption peak of N719 dye due to visible t_2 to π^* metal to ligand charge transfer. The quantum efficiency of the TiO_2-DSSC was about 33%, but this was increased to about 44% in the 1.0 wt % graphene TiO_2-DSSC. As a result, the quantum efficiency was increased to approximately 11%, which confirmed that the graphene-TiO_2 electrode induced more photons. Moreover, the measured IPCE values were broad over the entire wavelength range in graphene-TiO_2-DSSC. It represents that the larger amounts of dye molecules are adsorbed, and more light is transmitted through and scattered in the graphene-TiO_2 layer than in the TiO_2 photoelectrode.

Conclusions

We have synthesized graphene-linked TiO_2 in this study in which TiO_2 particles were evenly spiked on the surface of graphene nano-sheet. Graphene-linked TiO_2 materials were prepared to enhance the solar energy conversion efficiency. In comparing the performance with that of pure TiO_2, the 1.0 wt % graphene-TiO_2 DSSC showed superior solar energy conversion efficiency. In 100 $mWcm^{-2}$ simulated sunlight, the 1.0 wt % graphene-TiO_2 DSSC exhibited good performance with a solar energy conversion efficiency of approximately 6.05%, V_{oc} of 0.68 V, J_{sc} of 12.89 $mAcm^{-2}$, and FF of 0.69. The quantum efficiency of the graphene-DSSC was more enhanced by about 11% compared to that of TiO_2-DSSC. Additionally, the resistance was largely decreased in the cell assembled with the 1.0 wt % graphene-TiO_2-DSSC compared to that of the pure TiO_2-DSSC.

Acknowledgments. This work was supported by 2010 R&E program funded by the Korea Science Academy of Korea Advanced Institute of Science and Technology, for which the authors are very grateful.

References

1. Chae, J.; Kim, D. Y.; Kim, S.; Kang, M. *J. Ind. Eng. Chem.* **2010**, *16*, 906.
2. Lee, Y.; Chae, J.; Kang, M. *J. Ind. Eng. Chem.* **2010**, *16*, 609.
3. Ko, K. H.; Lee, Y. C.; Jung, Y. J. *J. Colloid Interf. Sci.* **2005**, *283*, 482.
4. Dhas, V.; Muduli, S.; Agarkar, S.; Rana, A.; Hannoyer, B.; Banerjee, R.; Ogale, S. *Sol. Energy* **2011**, *85*, 1213.
5. Curtiss, S.; Kovash, Jr.; Hoefelmeyer, D. J.; Logue, B. A. *Electrochimica Acta* **2012**, *67*, 18.
6. Stankovich, S.; Dikin, D. A.; Piner, R. D.; Kohlhaas, K. A.; Kleinhammes, A.; Jia, Y.; Wu, Y.; Nguyen, S. B. T.; Ruoff, R. S. *Carbon* **2007**, *45*, 1558.
7. Wang, X.; Zhi, L.; Mullen, K. *Nano Lett.* **2008**, *8*, 323.
8. Zhou, K.; Zhu, Y.; Yang, X.; Li, C. *New J. Chem.* **2010**, *34*, 2950.
9. Zhang, X.; Sun, Y.; Cui, X.; Jiang, Z. *Inter. J. Hydrogen Energy* **2012**, *37*, 811.
10. Li, Z.; Chen, Y.; Du, Y.; Wang, X.; Yang, P.; Zheng, J. *Inter. J. Hydrogen Energy* **2012**, *37*, 4880.
11. Hou, C.; Zhang, Q.; Li, Y.; Wang, H. *J. Hazard. Mater.* **2012**, *205*, 229.
12. Wu, J.; Shen, X.; Jiang, L.; Wang, K.; Chen, K. *Appl. Surf. Sci.* **2012**, *256*, 2826.
13. Ng, Y. H.; Iwase, A.; Bell, N. J.; Kudo, A.; Amal, R. *Catal. Today* **2011**, *164*, 353.
14. Yeo, M.-K.; Kang, M. *Water Res.* **2006**, *40*, 1906.
15. Hu, H.; Wang, X.; Wang, J.; Liu, F.; Zhang, M.; Xu, C. *Appl. Surf. Sci.* **2011**, *257*, 2637.
16. Choi, H.-J.; Kang, M. *Inter. J. Hydrogen Energy* **2007**, *32*, 3841.
17. Tauc, J. *Amorphous and Liquid Semiconductors*; Plenum Press: New York, 1974; p 171.
18. Chae, J.; Kang, M. *J. Power Sources* **2011**, *196*, 4143.
19. Shen, Q.; Sato, T.; Hashimoto, M.; Chen, C.; Toyoda, T. *Thin Solid Films* **2006**, *499*, 299.